ARCHIVES OF ELECTRICAL ENGINEERING VOL. 73(4), pp. 1087–1101 (2024)

DOI 10.24425/aee.2024.152112

Comparative view of coercivity mechanisms in soft and hard magnetic materials

MARCOS FLAVIO DE CAMPOS ✉, JOSÉ ADILSON DE CASTRO

PPGEM – EEEIMVR – UFF Universidade Federal Fluminense
Av dos Trabalhadores 420 Vila Santa Cecilia – Volta Redonda RJ 27255-125 – Brazil
e-mail: {✉ marcosflavio/joseadilsoncastro}@id.uff.br

(Received: 26.03.2024, revised: 24.11.2024)

Abstract: The main differences between soft and hard magnetic materials are commented on. It is discussed how the coercivity mechanisms can be affected by the domain wall energy. A spherical cap nucleus is used for this analysis. There is a competition between magnetostatic energy and domain wall energy terms. As a consequence, for soft magnetic materials, the magnetostatic energy term is dominant over the domain wall energy term. An explanation for the dependence of the coercivity with grain size is presented. For grain size above the single domain size, in hard magnetic materials with high magnetocrystalline anisotropy, the coercivity decreases following a law proportional to the inverse of the square root of the grain size, whereas in soft magnetic materials, the coercivity reduces proportionally to the inverse of grain size.

Key words: coercivity, hard magnetic materials, magnets, soft magnetic materials

1. Introduction

The origin of the coercivity in hard and soft magnetic magnets can be very different. Here, in this study, it is given a comparative view of these coercivity mechanisms. Wohlfarth [1] defines hard magnetic materials as those with coercivity above 100 Oe in CGS (7957. 75 A/m in SI). CGS means centimeter-gram-second whereas SI means System International). A detailed explanation of both systems, and their advantages and disadvantages are given in the Appendix.

The domain wall energy and domain wall thickness could be used for defining soft behavior. For example, an ideal soft magnetic material would have null domain wall energy and infinite domain wall thickness. However, this simple criterion fails when shape anisotropy is considered, as

in the case of Alnico magnets, where shape anisotropy can produce large coercivities of the order of 1–2 kOe (79577.5–159155 A/m) [1, 2]. This article presents a criterion based on the evaluation of magnetostatic and domain wall energies to separate between "soft" and "hard" behavior. This criterion excludes shape anisotropy, but it should be regarded that for shape anisotropy the phase must be of single-domain particle size.

It is not easy to apply this criterion to alpha-iron because the single-domain particle size is only ~ 15 nm [3, 4]. Besides, the hard phase should be embedded in a non-magnetic phase. This is the case of Alnicos [5–7]. Thus, the present discussion does not apply to Alnicos and shape anisotropy, which were addressed elsewhere [6, 7].

For soft magnetic materials, the intrinsic coercivity (*Hci*) and the coercivity (*Hc*) are almost the same. However, for hard magnetic materials the intrinsic coercivity *Hci* or *iHc* is higher than (much above) the coercivity *Hc* [8]. Both terminologies (*Hci* and *iHc*) are used in this paper. *Hci* comes from the curve $4\pi M_s \times H$ (CGS) whereas *Hc* comes from the curve $B \times H$ (CGS) [8, 9]. From the magnetic material point of view, the relevant curve is $4\pi M_s \times H$, whereas for electrical engineers, the most relevant curve, in many cases, is the curve $B \times H$ (especially for machine designing). A long list of abbreviations explaining *Hc*, *Hci*, and other indexes of merit in magnets is given in Reference [9].

Constantinides defines semi-hard magnets [10, 11] as those with intrinsic coercivities between 25 and 700 Oe (1989 to 55704 A/m) [11, 12]. These semi-hard magnetic materials include martensitic steels (thus nanocrystalline) and iron-based alloys with coercivity due to shape anisotropy. The semi-hard materials based on bcc iron (alpha iron) probably have grain size or particle size below the single domain particle size.

It was noted in our previous studies that the low initial susceptibility of the initial magnetization curve found in SmCo 2:17 type magnets (SmZrFeCoCu) and melt-spun NdFeB magnets is because the grain size is below the single domain size [13, 14].

2. Energy considerations

A spherical cap is defined in Fig. 1. The volume of that spherical cap is given by Eq. (1). The area is given in Eq. (2), and its energy is given in Eq. (3) for a flat wall. A_{wall} is a domain wall area and γ_D is the domain wall energy. The magnetostatic energy can be calculated as a function of x, as given by Eq. (4) and Eq. (6) [15–19], where $z = 1 - x$ (Eq. 4(b)). $Pn(z)$ represents Legendre polynomials with the index n. The sum of both energies is given by Eq. (6). The domain wall energy is calculated according to Eq. (6), where M_s is the magnetization of saturation. R_c is the single domain critical radius, as defined by Kittel [20]. R is the grain size radius. Figure 2 presents a plot of Eq. (6), Eq. (4) and Eq. (3) for three different situations: $R = 1/3R_c$, $R = R_c$ and $R = 3R_c$. When $R = 1/3R_c$, there is no minimum of energy in the curve $E_{\text{sum}}(x)$, the maximum is for $x = 0$, and this implies that the reversal of magnetization will happen by coherent rotation or the Stoner–Wohlfarth (SW) mode. However, for $R = 3R_c$, there is a minimum of energy (for $x/R = 1$), and this can enable a nucleation process using Eq. (7) [19], where theta is an angle between the applied field and crystal easy axis. Equation (7) represents the pressure exerted by the applied field H in a flat domain wall for the domain wall displacement.

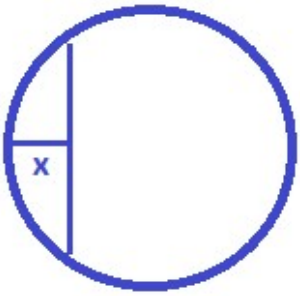

Fig. 1. Spherical cap near the surface of grain, defined by means of variable x

It is assumed the material is uniaxially anisotropic. The nucleus will occur at a spherical cap [17–19].

$$V(x) = \pi R x^2 - \frac{\pi}{3} x^3, \tag{1}$$

$$A_{\text{wall}} = \pi(2Rx - x^2), \tag{2}$$

$$E_{\text{wall}} = \pi(2Rx - x^2)\gamma_D, \tag{3}$$

$$E_{\text{magnetostatic}} = \frac{1}{2}\left(z\frac{(3 - z^2)}{3}\right)^2 + \sum_{n=2}^{\infty} \frac{n\left((n+1)c_n^2\right)}{(2n+1)^2}, \tag{4}$$

where:

$$c_n = \frac{P_{n-2}(z) - P_n(z)}{2n - 1} - \frac{P_n(z) - P_{n+2}(z)}{2n + 3}, \tag{4a}$$

$$z = 1 - x, \tag{4b}$$

$$E_{\text{sum}} = E_{\text{magnetostatic}} + E_{\text{wall}}, \tag{5}$$

$$\gamma_D = (4\pi/9)\, R_c M_s^2, \tag{6}$$

$$H(x) = \frac{1}{\cos\theta}\frac{1}{2M_s}\frac{1}{A_{\text{wall}}}\frac{\partial E(x)}{\partial x}. \tag{7}$$

The magnetostatic energy is proportional to M_s^2, whereas E_{wall} is proportional to γ_D. As can be seen in Table 1, the domain wall energy is two orders of magnitude higher for $SmCo_5$ when compared with alpha-iron, but M_s of $SmCo_5$ is almost half as much. In a soft magnetic material, the domain wall energy is low, so Eq. (2) is small if compared with the magnetostatic energy term. This detail can be used for the definition of hard and soft magnetic behavior. Table 1 is based on previous studies [21, 22] and from literature data [23]. Kittel domain theory [20] assumes negligible domain wall thickness and, thus, is very suitable for hard phases, i.e., phases with a high anisotropy field. Figure 2 gives the calculated energies, according to Eq. (6).

The variable x is defined in Fig. 1. Normalized Energy is non-dimensional and it is $E/4\pi^2 M_s^2 R^3$. The system used is CGS, there $N = 4\pi/3$ (the demagnetization factor of a sphere). Therefore, $E_{\text{sphere}} = 1/2NM_s^2(4\pi/3)R^3 = (2/9)4\pi^2 M_s^2 R^3$.

Table 1. Domain wall energy, magnetization of saturation and anisotropy field for some compounds in CGS and SI

Phase	**Domain wall energy γ (ergs/cm^3) or 10^{-1} J/m^3**	**Magnetization of saturation $4\pi M_s$ (kG) or $\mu_0 M_s$ (10^{-1}Tesla)**	**Anisotropy field H_A (kOe) or $\mu_0 H_A$ (10^{-1}Tesla)**
bcc iron 180° domain wall	1.2	21.7	–
$BaFe_{12}O_{19}$	9	4.8	16
$SrFe_{12}O_{19}$	8	4.8	19.5
$Nd_2Fe_{14}B$	27	16	77
Sm_2Co_{17}	43	12.5	70
$SmCo_5$	120	11.4	520

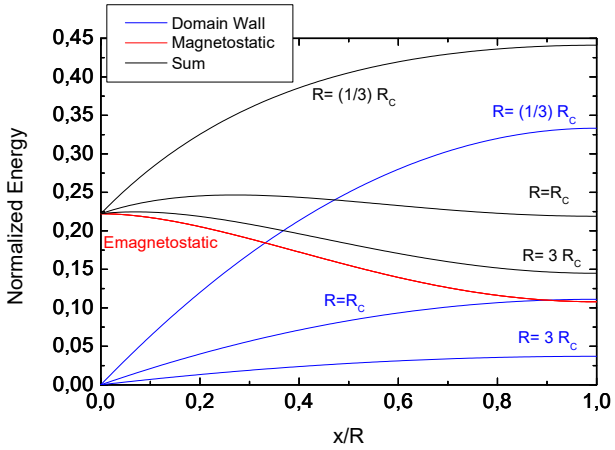

Fig. 2. Energies as function of x/R for three different cases: $R = 1/3R_c$, $R = R_c$ and $R = 3R_c$

3. Particle size below the single domain size

When the grain size is very small, much below the single domain size, the coercivity can decrease, due to thermal fluctuation effects [24]. There is a formula by Kneller and Luborsky [25], derived from the evaluation of energy barriers using the Stoner–Wohlfarth model, Eqs. (8), (9) and (10). The angle between M_s and the easy axis is ξ. The Kneller–Luborsky model [25] is given by Eq. (11) and Eq. (12). V_p is defined in Eq. (11), where k is the Boltzmann constant T is the temperature and K_1 is the first-order anisotropy constant. R_p is the particle radius, found with $V_{\text{sphere}} = 4/3\pi R^3$. *Hci* is the coercive field.

$$E = V(K_1 \sin^2 \xi + HM_s \cos \xi), \tag{8}$$

$$\Delta E = K_1 V \left(1 - \frac{HM_s}{2K_1}\right)^2, \tag{9}$$

$$\Delta E = K_1 V \left(1 - \frac{HciM_s}{2K_1}\right)^2 = 25kT, \tag{10}$$

$$V_p = \frac{25kT}{K_1}, \tag{11}$$

$$Hci = 1 - \left(\frac{V_p}{V}\right)^{1/2} = 1 - \left(\frac{R_p}{R}\right)^{3/2}. \tag{12}$$

4. Differences between soft and hard magnetic materials

For soft magnetic materials, coercivity is additive: It is the sum of different effects such as grain size, inclusions, and plastic deformation, as can be seen in Eq. (13) [26–29]. It has been mentioned [30] that the comparison between Eq. (13), Eq. (14) and Eq. (15) can be useful for non-destructive evaluation by magnetic methods. The permeability also can be an "additive" property, but especially for the initial permeability there is a relationship $\mu_i \sim 1/Hc$, thus it is inversely proportional to the coercive field.

$$Hc_{\text{Total}} = Hc_{\text{dislocations}} + Hc_{\text{grain size}} + Hc_{\text{inclusions}}, \tag{13}$$

$$\sigma_{\text{Total}} = \sigma_{\text{dislocations}} + \sigma_{\text{grain size}} + \sigma_{\text{inclusions}}, \tag{14}$$

$$\mu_i = 1/(Hc_{\text{dislocations}} + Hc_{\text{grain size}} + Hc_{\text{inclusions}}). \tag{15}$$

There are several striking differences between soft and hard magnetic materials, as discussed previously [19, 31]. A very brief summary will be given under points (i), (ii), (iii), (iv) and (v).

1. phases suitable for hard magnetic materials present only one magnetization axis, whereas soft phases have several easy axes, such as bcc iron with 3 easy axes at the [100] direction and fcc Nickel, as well as 4 easy axes at the [111] direction.
2. For hard magnetic materials, lattice defects decrease the coercivity. For soft magnetic materials, lattice defects increase the coercivity.
3. Above the single domain particle size: For hard magnetic materials, the coercivity mechanism is nucleation. For soft magnetic materials, the coercivity mechanism is pinning.
4. Another relevant difference is that for soft magnetic materials, coercivity decreases. $Hci \sim 1/R$ and for hard magnetic materials decreases according to $Hci \sim 1/R^{0.5}$. This question will be discussed in the next sections.
5. The classical pinning is caused by inclusions, and one can see that the coercivity is of the order of Oersteds in this case [32]. However, a coercivity of the order of kilo-Oersteds is explained with coherent rotation [1] or nucleation [18, 19] as a mechanism.

5. Nucleation in phase transformation theory

The name nucleation was earlier used by Volmer and Weber [33, 34]. The classical nucleation theory of phase transformations [33, 34] discusses a competition between a volume energy term and surface energy term. Here, E_V (Eq.16) denotes volume energy and E_s (Eq.17) is surface energy, a_V is a constant related to volume, and a_S is a constant related to surface energy. The

addition of Eq. (16) and Eq. (17) is represented by Eq. (18). r is the radius of the nucleus. From this simple model, a critical radius $r*$ is found that gives the rise to the nucleation process, see Fig. 3. The reversal of magnetization in particles above the single domain particle size can be considered an analogous situation. There is significant similarity between the set of equations, Eqs. (3), (4) and (6) and Eqs. (16), (17) and (18).

$$E_V = -a_V \frac{4}{3}\pi r^3, \tag{16}$$

$$E_S = a_S 4\pi r^2, \tag{17}$$

$$E_V + E_S = -a_V \frac{4}{3}\pi r^3 + a_S 4\pi r^2. \tag{18}$$

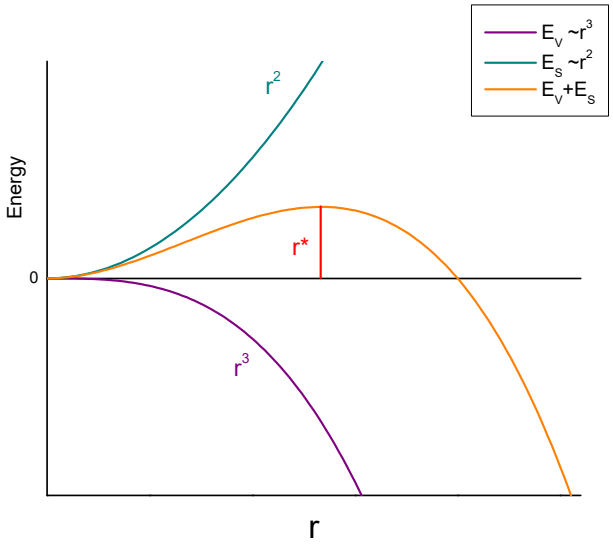

Fig. 3. Definition of the critical radius for nucleation

6. Effect of grain size on hard coercivity materials

A model for the effect of grain size on coercivity can be formulated based on a simple energy analysis. The starting point is the Stoner–Wohlfarth model. There are only two possibilities for the SW model: magnetized in one direction (Point A) or in the opposite direction (Point B), see Fig. 4. However, when the grain is larger than the single domain size, then other situations of minimum energy appear in the system, represented by points C and D (see Fig. 4), which can be identified with the coercive field. The SW model is only valid for single-domain size particles. How to extend the SW model to multidomain size particles?

A very simple possibility emerges from the scheme of Fig. 5. Here the variables α, β, c, cte, c_1, c_2 denote constants.

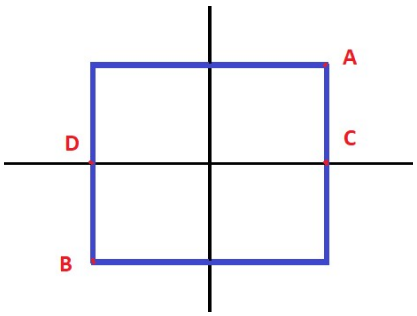

Fig. 4. Hysteresis showing points A, B, C and D

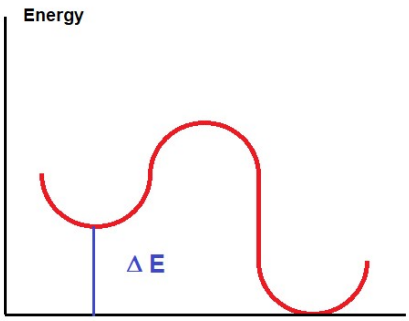

Fig. 5. Scheme showing variation of energy. The abscissa is time

Starting from Eq. (19), a simple energy balance results in Eqs. (20–22). The term $N_{\text{grain}}M_s$ of Eq. (19) becomes $\beta(\Delta E/M_s)$ in Eq. (20). iHc is the intrinsic coercivity. Equation (32) has two adjusting coefficients (c_1, c_2). It is found that experimental results for hard ferrites [35] and NdFeB [36] are well described by the law given by Eq. (22).

$$iHc = \alpha H_A - N_{\text{grain}} M_s, \tag{19}$$

$$iHc = \alpha H_A - \beta \frac{\Delta E}{M_s}, \tag{20}$$

$$\Delta E = \frac{1}{2} N M_s^2 - cte \frac{\sqrt{\gamma_D M_s^2}}{\sqrt{R}} = c\left(\frac{M_s \sqrt{\gamma}_D}{\sqrt{R}_c} - \frac{M_s \sqrt{\gamma}_D}{\sqrt{R}}\right), \tag{21}$$

$$iHc = c_1 - \frac{c_2}{\sqrt{R}}. \tag{22}$$

The model of Eqs. (19–22) only compares energies, and does not give any indication about the physics behind the process, or how it happens.

There are different models: one given by Eqs. (3), (4), (6), (16), (17) and (18) and another by Eqs. (19–22). Are these models related? The next section will address this question.

7. The nucleation model

As a possible first approximation, the variation of magnetostatic energy due to domain wall formation can be assumed near zero (i.e. Δ Emagnetostatic$\sim$ 0 for very small x). ΔE_{wall} is given by Eq. (3). Thus Eq. (3) can be compared with Eq. (9), resulting in Eq. (23). After some algebraic calculations, Eqs. (24) and (25) are obtained. H of Eq. (25) can be identified as the coercive field. Eq. (23) emphasizes the relevance of the domain wall energy, which can be several orders of magnitude higher for a hard phase, as aforementioned.

$$K_1 V_{\text{barrier}} \left(1 - \frac{H}{H_A}\right)^2 = \pi(2Rx - x^2)\gamma_D, \tag{23}$$

$$\frac{H}{H_A} = 1 - \left(\frac{\pi(2Rx - x^2)\gamma_D}{K_1 V_{\text{barrier}}}\right)^{1/2}, \tag{24}$$

$$H = H_A - H_A\sqrt{\frac{\gamma_D}{K_1}}\left(\frac{A_{\text{wall}}}{V_{\text{barrier}}}\right)^{1/2}. \tag{25}$$

There is a relationship between Eqs. (1) and (2), given by Eq. (26).

$$A_{\text{wall}} = \frac{\mathrm{d}}{\mathrm{d}x}V(x) = \pi 2Rx - \pi x^2. \tag{26}$$

If it is considered that $V_{\text{barrier}} \sim R\text{^}3$ and $A_{\text{wall}} \sim R\text{^}2$ then Eq. (27) has a format similar to Eq. (22), and gives a theoretical explanation for the experimental coefficients (c_1, c_2). One of the problems in understanding coercivity is that lattice defects can locally affect the activation volume [19]. Thus, the effect of lattice defects corresponds to that of reducing the activation volume, here represented by η in Eq. (27). Previously α multiplying H_A was introduced (see Eq. 19), and another possibility is the alteration given by Eq. (28).

$$H = H_A - H_A\sqrt{\frac{\gamma_D}{\eta K_1}}\left(\frac{1}{R}\right)^{1/2}, \tag{27}$$

$$H = \alpha H_A - \alpha H_A\sqrt{\frac{\gamma_D}{\eta K_1}}\left(\frac{1}{R}\right)^{1/2}. \tag{28}$$

8. The one domain wall model

The model presented in this section is for soft magnetic materials. The model described in this section assumes that the domain wall already exists [37]. This is possible since the domain wall energy is much lower than the magnetostatic energy when comparing Eqs. (3), and (4). In other words, for a soft phase, the domain wall is easily formed, and because of its formation, it does not require a significant amount of energy as in hard phases. For the calculation, it is assumed grain size is slightly above the single domain size in such a way that there is only one domain wall. This situation can be found in soft ferrites [38, 39].

When a domain wall is in half of the sphere, see Fig. 6, the magnetostatic energy is reduced by approximately half. A field can move and thus eliminate this domain wall of Fig. 6 given by Eq. (29).

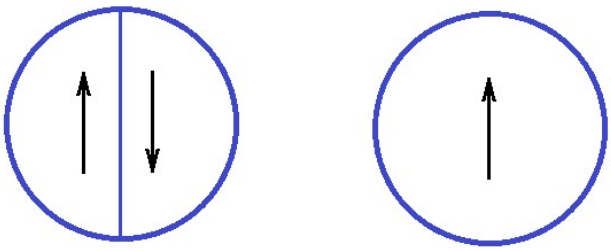

(a) (b)

Fig. 6. Spherical grain: (a) with one domain wall; (b) without domain wall, magnetized in one direction. Schematic

Equation (29) is a force balance equation. In this process, domain wall energy is consumed, resulting in the following relationship: Energy = Area = $4M_sH = (2\gamma\pi R^2/(4/3)\pi R^3)$, see Eq. (30). Equation (30) is an energy balance equation.

$$H = \frac{1}{\cos\theta}\frac{1}{2M_s}\frac{3}{2}\frac{\gamma_D}{R}, \tag{29}$$

$$H = \frac{3}{8}\frac{\gamma}{RM_s}, \tag{30}$$

$$H_c = \frac{3\gamma}{8RM_s}\left(\frac{2}{\cos\theta} + 1\right). \tag{31}$$

In Eq. (31), for the bcc structure with an easy axis at [100] direction, and a hard axis at the [111] direction, in the case of iron or silicon steels, $0 \leq \theta \leq \arccos(1/\sqrt{3})$. Nickel is fcc, with an easy axis in the direction [111], and it corresponds to 4 easy axes [40]. The domain wall displacement takes place parallel to the easy axis that is nearest to the direction of the applied field, as can be seen in Fig. 6(a).

The sum of the two equations, Eqs. (29) and (30), gives the coercive field H_c due to grain size, see Eq. (31). This explains the law $Hc \sim 1/R$, which is mentioned by Cullity and Graham [24] as purely experimental. Globus and Guyot [31] presented a very similar idea to Eq. (31). However, Globus and Guyot did not discuss the angular dependence of coercivity [41]. Equation (31) gives a result similar to that experimentally found by Mager [42]. Equation (31) can be extended for larger grain size, i.e. it is also valid for $R \ll Rc$ because it gives the necessary field for domain wall moving. Equation (31) has no adjusting coefficients and can be directly compared with experimental results.

9. Angular dependence of coercivity

According to Rowlands [43], the competition between magnetostatic and exchange energy terms can lead to relationships such as $Hc \sim 1/R^{0.5}$ or $Hc \sim 1/R$. As discussed earlier, in Eq. (6), if $E_{\text{magnetostatic}}$ is dominant, $Hc \sim 1/R$ is observed, as in Eq. (31). Instead, if the domain wall energy is high, the term E_{wall} is dominant, then $Hc \sim 1/R^{0.5}$ is found, as in Eq. (22) or Eq. (28).

$$K_1 V_{\text{barrier}}\left(1 - \frac{H}{H_A}\right)^2 = \Delta E_{\text{wall}}. \tag{32}$$

In Eq. (23), it was assumed that the applied field H was parallel to the crystal easy axis. Equation (23) is now rewritten as Eq. (32) to emphasize the energy variation. Equation (32) also allows one to discuss the angular dependence of coercivity. The left-hand term in Eq. (32) is an SW term and follows the SW angular dependence given by Eqs. (33) and (34) and depicted in Fig. 7 [44]. The right-hand term of Eq. (32) will give rise to a Kondorsky term (1/cos theta term), as can be seen in Eq. (3) and Eq. (7). The explanation for the competition between SW angular dependence and Kondorsky angular dependence is given in Fig. 1: for $R < Rc$, the reversal takes place by coherent rotation, see Eqs. (33) and (34). For $R > Rc$, more relevant becomes the domain wall displacement process, and the coercivity will tend to follow the 1/cos theta law, as in Eq. (7). This can explain the experimental observations for barium ferrite [45] and NdFeB magnets [46,47].

$$h_c = \frac{(1 - t^2 + t^4)^{1/2}}{1 + t^2}, \tag{33}$$

$$t = (\tan\theta)^{1/3}. \tag{34}$$

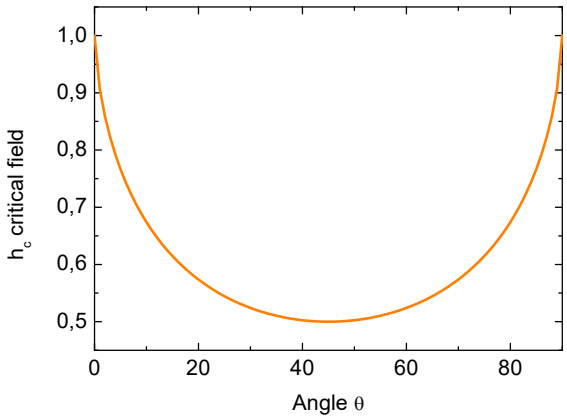

Fig. 7. Reduced field h_c as function of an angle θhc denotes the field for inversion of magnetization, according to the SW model

For coercivity analysis, however, the relevant detail is the maximum of the derivative $dE(x)/dx$ [48]. Thus Eq. (7) becomes Eq. (35) for coercivity predictions; and it follows that Hci is given by Eq. (35) for pure domain wall displacement.

$$Hci = \frac{1}{\cos\theta}\frac{1}{2M_s}\frac{1}{A_{\text{wall}}}\left(\frac{\partial E(x)}{\partial x}\right)_{\max}. \tag{35}$$

Thus, SW processes and domain wall displacement processes compete: the winner will be the process that spends less energy. For phases with only one easy magnetization axis, if $\theta \to \pi/2$, then in Eq. (35) $Hci \to \infty$, but this does not happen because in this case ($\theta = \pi/2$) the reversal of magnetization happens by SW mode. This illustrates how complex is this analysis, and the effect of lattice defects makes the problem even more complicated, as discussed in the previous study [49]. The present study used the CGS system of units [50–52], as discussed in the Appendix.

10. Conclusions

It is discussed how coercivity mechanisms can be affected by the domain wall energy. A spherical cap nucleus is used for this analysis. There is a competition between magnetostatic energy and domain wall energy terms. As a consequence, for soft magnetic materials, the magnetostatic energy term is dominant over the domain wall energy term.

An explanation for the dependence of coercivity on different grain sizes is presented. For grain size above the single domain size, in hard magnetic materials with high magnetocrystalline anisotropy, the coercivity decreases following a law proportional to the inverse of the square root of the grain size, whereas in soft magnetic materials, the coercivity reduces proportionally to the inverse of the grain size. Thus, if $E_{\text{magnetostatic}}$ is dominant, a $Hc \sim 1/R$ relationship is observed. Instead, if E_{wall} is dominant, a $Hc \sim 1/R^{0.5}$ relationship is found.

Appendix

Here, it will be given a brief explanation of the main differences between CGS and SI, the most used systems of units for magnetic materials. Old articles from the 1940s, 1950s and 1960s, such as those written by Edmund Stoner, Charles Kittel and Louis Neel, typically employed CGS. Nevertheless, recent papers have preferred the SI. In CGS, the vacuum permeability is defined as 1, whereas in SI, the vacuum permeability is $4\pi\ 10^{-7}$ Tesla meter/Ampere. This is a very relevant difference.

In CGS (emu), or Amperian CGS, we have Eq. (A.1) with B and M expressed in Gauss (G), and the applied field H expressed in Oersteds (Oe). On the other hand, in SI (MKS, Kennelly convention), the equation relating the applied field (H), magnetization (M) and induction (B) is given by Eq. (A.2) with B and J expressed in Tesla (T) and the field H is expressed in Ampere/meter (A/m). J is the polarization of saturation.

$$B = H + 4\pi M, \tag{A.1}$$

$$B = \mu_o H + J \quad \text{or} \quad B = \mu_o(H + M). \tag{A.2}$$

An obvious disadvantage of SI (Eq. (A.2)) is the presence of the dimensional constant μ_0. Instead, the CGS has a simpler definition for permeability, $\mu = B/H$. For the SI MKS Kennelly, the relative permeability (μ_R) is given by $\mu_R = B/\mu_0 H$, and here μ_R is non-dimensional. Then, there is another permeability $\mu = \mu_0\mu_R$. Therefore, in the CGS there is only one permeability, but in the SI MKS Kennely, there are three different permeabilities, which may cause confusion. This detail makes the CGS, in general, more interesting than SI for the experimentalist. However, from the physics point-of-view, the SI MKS Kennely is more interesting because Eq. (A.3), which is a result first obtained by James C. Maxwell, who indicated that light is, in fact, an electromagnetic wave. c is the speed of light in the vacuum, and ε_o is the permittivity in free space, with $c = 2.99810^8$ m/s. 1 Tesla = 1 weber/m^2 (Wb/m^2).

$$c = \frac{1}{\sqrt{\mu_0 \varepsilon_o}}. \tag{A.3}$$

The constant ε_o – the permittivity – is found in Eq. (A.4), where q_1 and q_2 are the charges (in coulombs, C); r is the distance between the charges (m); the force F is expressed in newtons, N).

In MKS, $\varepsilon_o = 10^7/4\pi\, c^2$ (F/m or farad per meter). In analogous manner, Eq. (A.5) gives the force between two magnetic poles m_1 and m_2 (weber) separated by the distance r (meters).

$$F = \frac{1}{4\pi\varepsilon_o}\frac{q_1 q_2}{r^2}. \tag{A.4}$$

$$F = \frac{1}{4\pi\mu_o}\frac{m_1 m_2}{r^2}. \tag{A.5}$$

In CGS (emu), the energy is expressed as in Eq. (A.6), and in SI (MKSA, Kennelly) as in Eq. (A.7), where θ is the angle between the vectors M and H. The conversion between some units of CGS to SI (MKS, Kennelly) is given as 1 Oe = $10^3/4\pi$ A/m = 9.58 A/m, 1 G = 10^{-4} T (energy density), 1 erg/cm^3 = 10^{-1} J/m^3.

$$E = -MH\cos\theta, \tag{A.6}$$

$$E = -JH\cos\theta \quad \text{or} \quad E = -\mu_o MH\cos\theta. \tag{A.7}$$

A possible disadvantage of CGS would be the presence of the constant 4π in the equation $B = H + 4\pi M$. But this is questionable: the factor 4π should appear when the physical situation reflects spherical symmetry. If the system were rationalized (in this case the system is said to be rationalized [50]), the constant 4π would no longer appear in Maxwell's equations.

However, concerning the demagnetizing field N, SI is more interesting and less confusing than the CGS because $Nx + Ny + Nz = 1$ against $Nx + Ny + Nz = 4\pi$ in the CGS. Here, x, y and z denote 3 dimensional (3D) coordinates. Some cases are described bellow:

Sphere: $Nx = Ny = Nz = 1/3$ (SI MKS), and $Nx = Ny = Nz = 4\pi/3$ (CGS),

Cube: $Nx = Ny = Nz = 1/3$ (SI MKS), and $Nx = Ny = Nz = 4\pi/3$ (CGS),

Infinite cylinder: $Nz = 0$, $Nx = Ny = 1/2$ (SI MKS), and $Nz = 0$, $Nx = Ny = 2\pi$ (CGS),

Infinite sheet (thin film): $Nz = 1$, $Nx = Ny = 0$ (SI MKS), and $Nz = 4\pi$, $Nx = Ny = 0$ (CGS).

It is also worth noting that SI (MKS) is not always considered disadvantageous by the experimentalist when compared to CGS. For example, in the case of equations mixing magnetic and electrical phenomena (such as the eddy loss equation), SI (MKS) tends to be more suitable.

References

[1] Wohlfarth E.P., *Hard magnetic materials*, Advances in Physics, vol. 8, no. 30, pp. 87–224 (1959).

[2] Stoner E.C., *Ferromagnetism: magnetization curves*, Reports on Progress in Physics, vol. 13, no. 1, pp. 83–183 (1950).

[3] Amar H., *Size Dependence of the Wall Characteristics in a Two-Domain Iron Particle*, Journal of Applied Physics, vol. 29, no. 3, pp. 542–543 (1958), DOI: 10.1063/1.1723216.

[4] Amar H., *Magnetization Mechanism and Domain Structure of Multidomain Particles*, Physical Review, vol. 111, no. 1, pp. 149–153 (1958), DOI: 10.1103/PhysRev.111.149.

[5] Nesbitt E.A., Heidenreich R.D., *The magnetic structure of Alnico 5*, Electrical Engineering, vol. 71, no. 6, pp. 530–534 (1952), DOI: 10.1109/ee.1952.6437538.

[6] de Campos M.F., Romero S.A., da Silva L.M., de Castro J.A., *Shape Anisotropy and Magnetic Texture Determination in Anisotropic and Isotropic Alnico Magnets*, JOM (2024), DOI: 10.1007/s11837-024-06586-3.

[7] de Campos M.F., *Shape Anisotropy as Coercivity Mechanism*, Materials Science Forum, vol. 869, pp. 591–595 (2016), DOI: 10.4028/www.scientific.net/msf.869.591.

[8] Kumar K., *RETM5 and RE2TM17permanent magnets development*, Journal of Applied Physics, vol. 63, no. 6, R13–R57 (1988), DOI: 10.1063/1.341084.

[9] MMPA PMG-88, *Permanent Magnet Guidelines*, Magnetic Materials Producers Association, 11 South LaSalle Street, Suite 1400, Chicago, IL 60603 (1998), available at https://www.intemag.com/images/MMPAPMG-88.pdf.

[10] Stan Zurek, *Magnetic Materials*, available at https://www.e-magnetica.pl/doku.php/magnetic_materials.

[11] Constantinides S., *Semi hard magnets* (2017), https://www.arnoldmagnetics.com/wp-content uploads/2017/10/Semi-Hard-Magnets-Constantinides-Magnetics-2011-psn-hi-res.pdf.

[12] Bozorth R.M., *Ferromagnetism*, IEEE Press, Appendix 4, pp. 872–873 (1993).

[13] Romero S.A., Moreira A.J., Landgraf F.F.G., de Campos M.F., *Abnormal coercivity behavior and magnetostatic coupling in SmCoCuFeZr magnets*, Journal of Magnetism and Magnetic Materials, vol. 514, 167147 (2020), DOI: 10.1016/j.jmmm.2020.167147.

[14] de Campos M.F., de Castro J.A., *Calculation of Recoil Curves in Isotropic and Anisotropic Stoner–Wohlfarth Materials*, IEEE Transactions on Magnetics, vol. 56, no. 3, pp. 1–4, 7512304 (2020), DOI: 10.1109/TMAG.2019.2957147.

[15] Neel L., *Effet des cavites et des inclusions sur le champ coercitif*, Cah. Phys., vol. 25, pp. 21–44 (1944).

[16] Neel L., *Remarques sur la theorie des proprietes magnetiques des couches minces et des grains fins*, J. Phys Radium, vol. 17, no. 3, pp. 250–255 (1956).

[17] Coleman J.E., Carey R., *Magnetisation reversal of spherical particles containing a single plane domain boundary*, J. Phys. D: Appl. Phys., vol. 15, no. 3, pp. 473–486 (1982), DOI: 10.1088/0022-3727/15/3/013.

[18] de Campos M.F., de Castro J.A., *Nucleus Size Determination for Nd2Fe14B, Sm2Co17, SmCo5 and BaFe12O19 Magnets*, Materials Science Forum, vols. 727–728, pp. 151–156 (2012), DOI: 10.4028/www.scientific.net/msf.727-728.151.

[19] de Campos M.F., de Castro J.A., *An overview on nucleation theories and models*, Journal of Rare Earths, vol. 37, no. 10, pp. 1015–1022 (2019).

[20] Kittel C., *Theory of the Structure of Ferromagnetic Domains in Films and Small Particles*, Physical Review, vol. 70, nos. 11–12, pp. 965–971 (1946).

[21] Romero S.A., Rodrigues D., Jr., Germano T., Cohen R., de Castro J.A., de Campos M.F., *Coercivity mechanisms in nanocrystalline Sm–Co–Cu thin films: the spring effect*, Appl. Nanoscience, vol. 13, pp. 6353–6372 (2023).

[22] de Campos M.F., de Castro J.A., *Role of exchange energy on the relationship between coercivity and grain size: Application for hard ferrites*, Proceedings of the 27th International Workshop on Rare Earth and Future Permanent Magnets and their Applications, University of Birmingham Birmingham UK (3rd-7th September 2023), pp. P2-21-8 (2023).

[23] Kojima H., *Fundamental properties of hexagonal ferrites with magnetoplumbite structure*, In Handbook of Ferromagnetic Materials, Chapter 5, Edited by E.P. Wohlfarth, vol. 3, North-Holland Publishing Company, pp. 305–391 (1982).

[24] Cullity B.D., Graham C.D., Jr., *Introduction to Magnetic Materials*, 2nd Edition, Wiley, Hoboken, New Jersey, 361 (2009).

[25] Kneller E.F., Luborsky F.E., *Particle Size Dependence of Coercivity and Remanence of Single-Domain Particles*, J. Appl. Phys., vol. 34, pp. 656–658 (1963).

[26] Adler E., Pfeiffer H., *The influence of grain size and impurities on the magnetic properties of the soft magnetic alloy 47.5% NiFe*, IEEE Transactions on Magnetics, vol. 10, no. 2, pp. 172–174 (1974), DOI: 10.1109/tmag.1974.1058314.

[27] Pfeifer F., Radeloff C., *Soft magnetic Ni–Fe and Co–Fe alloys – some physical and metallurgical aspects*, Journal of Magnetism and Magnetic Materials, vol. 19, nos. 1–3, pp. 190–207 (1980), DOI: 10.1016/0304-8853(80)90592-2.

[28] Pfeifer F., Kunz W., *Bedeutung von kornstruktur und fremdkörpereinschlüssen für die magnetisierungseigenschaften hochpermeabler Ni–Fe-legierungen*, Journal of Magnetism and Magnetic Materials, vol. 4, nos. 1–4, pp. 214–219 1977, DOI: 10.1016/0304-8853(77)90038-5.

[29] Kunz W., Pfeifer F., *The Influence of Grain Structure and Nonmagnetic Inclusions on the Magnetic Properties of High-Permeability Fe-Ni-Alloys*, AIP Conference Proceedings (1976), DOI: 10.1063/1.2946158.

[30] de Campos M.F., *Achievements in micromagnetic techniques of steel plastic stage evaluation*, Advances in Materials Science, vol. 20, no. 1, pp. 16–55 (2020), DOI: 10.2478/adms-2020-0002.

[31] de Campos M.F., *Coercivity Mechanism in Hard and Soft Sintered Magnetic Materials*, Materials Science Forum, vol. 802, pp. 563–568 (2014), DOI: 10.4028/www.scientific.net/msf.802.563.

[32] de Campos M.F., Emura M., Landgraf F.J.G., *Consequences of magnetic aging for iron losses in electrical steels*, Journal of Magnetism and Magnetic Materials, vol. 304, pp. e593–e595 (2006).

[33] Volmer M., Weber A., *Keimbildung in übersättigten Gebilden*, Zeitschrift Für Physikalische Chemie, vol. 119, no. 1, pp. 277–301 (1926).

[34] Volmer M., *Kinetics of Phase Formation* (*Kinetik der Phasenbildung*) (English translation) (1939), Available at: https://apps.dtic.mil/sti/citations/tr/ADA800534.

[35] de Campos M.F., Sampaio da Silva F.A., Romero S.A., de Castro J.A., *Hysteresis Modelling and Coercivity Mechanisms in Hard Ferrites*, In 14th International Symposium on Linear Drivers for Industry Applications (LDIA), pp. 28–30 (2023), DOI: 10.1109/LDIA59564.2023.10297507.

[36] de Campos M.F., *Effect of Grain Size on the Coercivity of Sintered NdFeB Magnets*, Materials Science Forum, vols. 660–661, pp. 284–289 (2010).

[37] de Campos M.F., *A General Coercivity Model for Soft Magnetic Materials*, Materials Science Forum, vols. 727–728, pp. 157–162 (2012).

[38] van der Zaag P.J., *New views on the dissipation in soft magnetic ferrites*, Journal of Magnetism and Magnetic Materials, vols. 196–197, pp. 315–319 (1999).

[39] Aarts J., Abu Shiekah I., van der Zaag P.J., *Domain structure in polycrystalline MnZn ferrite imaged by magnetic force microscopy*, Journal of Applied Physics, vol. 85, no. 10, pp. 7302–7309 (1999).

[40] Kaya S., Masiyama Y., *The Magnetic Properties of Single Crystals of Nickel*, Nature, vol. 120, pp. 951–952 (1927), DOI: 10.1038/120951a0.

[41] Guyot M., Globus A., *Determination of domain wall energy and the exchange constant from hysteresis in ferromagnetic polycrystals*, J. Physique Colloque C1, vol. 38, pp. C1-157–C1-162 (1977).

[42] Mager A., *Über den Einfluß der Korngröße auf die Koerzitivkraft*., Ann. Phys. Lpz., vol. 446, no. 1, pp. 15–16 (1952).

[43] Rowlands G., *The variation of coercivity with particle size*, Journal of Physics D: Applied Physics, vol. 9, no. 8, pp. 1267–1269 (1976).

[44] de Campos M.F., de Castro J.A., *Predicting Recoil Curves in Stoner–Wohlfarth Anisotropic Magnets*, Acta Physica Polonica A, vol. 136, no. 5, pp. 737–739 (2019).

[45] Ratnam D.V., Buessem W.R., *Angular Variation of Coercive Force in Barium Ferrite*, Journal of Applied Physics, vol. 43, no. 3, pp. 1291–1293 (1972), DOI: 10.1063/1.1661260.

[46] Martinek G., Kronmüller H., *Influence of grain orientation of the coercive field in Fe-Nd-B permanent magnets*, Journal of Magnetism and Magnetic Materials, vol. 86, nos. 2–3, pp. 177–183 (1990).

[47] Katter M., *Angular dependence of the demagnetization stability of sintered Nd-Fe-B magnets*, IEEE Transactions on Magnetics, vol. 41, no. 10, pp. 3853–3855 (2005).

[48] Chen C.W., *Magnetism and Metallurgy of Soft Magnetic Materials*, North-Holland Publishing Company: Elsevier North-Holland, 129 (1977).

[49] de Campos M.F., *Effect of Grain Size, Lattice Defects and Crystalline Orientation on the Coercivity of Sintered Magnets*, Materials Science Forum, vols. 530–531, pp. 146–151 (2006), DOI: 10.4028/www.scientific.net/msf.530-531.146.

[50] Kennelly A.E., *Rationalised versus Unrationalised Practical Electromagnetic Units*, Proceedings of the American Philosophical Society, vol. 70, no. 2, pp. 103–119 (1931).

[51] *The Giorgi System of Units*, Nature, 134, 283 (1934), available at https://www.nature.com/articles/134283b0.

[52] Goldfarb R.B., *Electromagnetic Units, the Giorgi System, and the Revised International System of Units*, IEEE Magnetics Letters, vol. 9, no. 1205905, pp. 1–5 (2018), DOI: 10.1109/LMAG.2018.2868654.